sciendo

POLISH MARITIME RESEARCH 3 (119) 2023 Vol. 30; pp. 142-152
10.2478/pomr-2023-0047

# DESIGN OF AN AUTONOMOUS IOT NODE POWERED BY A PEROVSKITE-BASED WAVE ENERGY CONVERTER

**Marcin Drzewiecki** *
**Jarosław Guziński**
Department of Electric Drives and Energy Conversion, Faculty of Electrical and Control Engineering, Gdańsk University of Technology, Poland

* Corresponding author: *marcin.drzewiecki@pg.edu.pl (M. Drzewiecki)*

**ABSTRACT**

*This paper presents the results of experimental research focused on wave energy harvesting and its conversion to power Internet of Things (IoT) devices. The harvesting and conversion process was performed using a wave energy converter (WEC) consisting of a lead zirconate titanate piezoelectric ceramic perovskite material and a prototype power electronic circuit. The designed WEC was considered as a power supply for an end node device (END) of an IoT network. The END consisted of a long-range radio module and an electronic paper display. A set of physical experiments were carried out, and the results confirmed that an energy surplus was supplied by WEC compared to the energy consumed by the END. Hence, the proposed scheme was experimentally validated as a convenient solution that could enable the autonomous operation of an IoT device. The use case presented here for the proposed WEC was analysed for selected sea areas on the basis of wave statistics. The novelty of this paper arises from an investigation that confirms that WECs can significantly contribute to the development of wireless and mobile IoT communication powered by freely available sea wave energy.*

**Keywords:** wave energy converter; renewable energy; internet of things; IoT applications; hydropower

## INTRODUCTION

Wave energy converters (WECs) are devices intended for harvesting the energy of water waves and converting it into a useful form. The first patent associated with the harvesting and use of wave energy dates back to the 18th century [1,2], and related to a solution for the harvesting of water wave energy and its conversion into a useful mechanical form. Since then, many patents and implementations regarding WEC have emerged, in regard to both model-scale laboratory conditions and full-scale sea conditions [3]. Solutions have also been proposed for harvesting the mechanical energy of water waves and converting it into electrical form, through the use of electrical machines operating as generators [4]. Since then, numerous considerations have been made regarding WEC, and such devices are still being developed [5,6]. Additional approaches in terms of applied materials and methods of harvesting and converting this energy into a useful electrical form have also been introduced over recent years [7,8]. The solutions described in these works show that for certain applications, electric machines that require maintenance can be replaced with maintenance-free piezoelectric materials (PMs) or dielectric elastomers (DEs). These materials generate electrical energy under the mechanical influence of water waves. The main motivation for the work described in the current paper, and its novelty compared to related works, is

an investigation of the possibility of harvesting the energy of water waves and converting it into electrical form via PMs, for use in powering distributed and autonomous elements of communication networks located onshore, nearshore, or offshore.

The concept of an integrated network consisting of software and hardware elements in which nodes received data packets at radio frequencies was formulated in an early paper in the 1990s [9]. In later works published in the 2000s, this concept began to be referred to as the Internet of Things (IoT) [10]. Over time, IoT solutions became more advanced [11], lower in power [12] and more common [13].

Both of the technologies described above, WEC and IoT, are still under development, and their role in meeting human needs is expected to grow significantly. If current trends continue [2,11], the use of WECs for the IoT is going to be one of the most essential aspects of sustainable development in the areas of wireless and mobile communication. A ceramic perovskite material called lead zirconate titanate (PZT) is applied in the present work. PZT was chosen due to its ability to convert mechanical energy into electrical form at low cost, its ease of operation, and its widespread availability [14]. The objectives and scope of this work were to design and validate a PZT-based WEC that was capable of powering IoT communication by harvesting freely available sea wave energy.

## ENERGY CONVERSION

The energy of water waves was discussed in [19]. Below is a study on the availability of mechanical wave energy when harvested and converted into electrical form. The energy of a water wave can be expressed as follows in the time domain and in the discrete frequency domain. The mechanical energy $E_A$ contained in a progressive sinusoidal water wave consists of potential energy $E_p$ and kinetic energy $E_k$. The amount of energy in such a wave per unit surface area of the water is given by Eq. (1) [15]:

$$E_A = E_p + E_k = \frac{1}{2}\rho g {z_A}^2 \tag{1}$$

where $\rho$ is the density of water and $g$ is the acceleration due to gravity. $z_A$ is the amplitude of the two-dimensional progressive sinusoidal wave, as shown in Fig. 1.

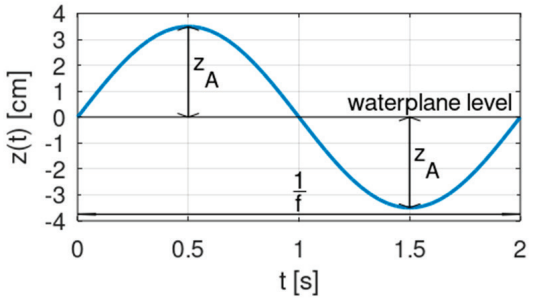


*Fig. 1. Two-dimensional progressive sinusoidal wave at the surface of the water [19].*

A water wave passing through an energy harvesting point in an area of water can be considered as a sum of two-dimensional progressive sinusoidal waves, as shown in Eq. (2) [16]:

$$z(t) = \sum_{i=1}^{\infty} z_{Ai} \cos\left(2\pi f_i t + \varepsilon_k\right) \tag{2}$$

where $z_{Ai}$ is the amplitude of the sinusoidal component with frequency $f_i$. The parameter εk is the phase of each component, and is randomly applied in the range of 0–2π to reflect the space-time randomness of the wave process in the area of water. The summation of the two-dimensional progressive sinusoidal waves given in Eq. (2) is illustrated in Fig. 2.

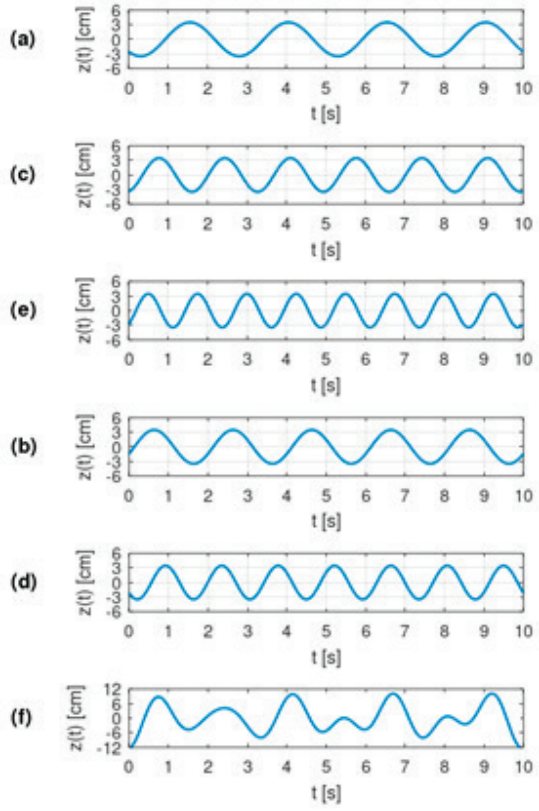


*Fig. 2. A water wave (f) can be considered as the sum of several two-dimensional progressive sinusoidal wave harmonics with amplitudes of 3.5 cm and frequencies of: (a) 0.4 Hz, (b) 0.5 Hz, (c) 0.6 Hz, (d) 0.7 Hz, (e) 0.8 Hz. [19]*

The energy $E$ contained per unit surface area of the water for the water waves formulated in Eq. (2) can be calculated using Eq. (3):

$$E = \frac{1}{2}\rho g \sum_{i=1}^{\infty} {z_{Ai}}^2 \tag{3}$$

The time domain mathematical model in Eq. (2) can be transformed into the frequency domain and expressed as harmonics with frequencies fi and amplitudes $z_{Ai}$. The model of waves on the surface of the water can be considered as a power spectrum of harmonics $S(f_i)$, as given in Eq. (4) [17]:

$$S(f_i) = \frac{A}{{f_i}^5} \exp\left(\frac{-B}{{f_i}^4}\right) \quad (4)$$

The values of $A$ and $B$ are determined based on the type [17] and state of the sea under consideration [18]. The energy $E(f_i)$ related to the power spectrum harmonics and expressed per unit surface area of the water can be represented in the frequency domain as:

$$E(f_i) = \rho g S(f_i) \quad (5)$$

The energy expressed above in the form of harmonics, which occurs naturally in areas of water, can be converted into a useful electrical form via the piezoelectric effect. The piezoelectric effect occurs in certain materials, including PZT, and involves the generation of an electric charge when the material is deformed [14]. Based on the physical definition of work, it can be considered that the harmonic energy expressed in Eq. (3) can be transferred to a floating body (e.g. a buoy) by applying a harmonic force $F_{Vi}$ along a vertical displacement $Z_{Ai}$ . The energy is transferred with efficiency $\eta_i$. Hence, the harmonic of the force vertical component $F_{Vi}$ per unit surface area of the water can be expressed as shown in Eq. (6):

$$F_{Vi} = \eta_i \frac{1}{2} \rho g z_{Ai} \quad (6)$$

When the energy is transferred by the further application of a harmonic force component $F_{Vi}$ from the buoy to the PZT, such that the force component points in the same direction as the polarisation of the PZT material, then the generated static voltage $V_{si}$ is given as shown in Eq. (7) [20]:

$$V_{Si} = \frac{g_{33} F_{Vi} t}{C} \quad (7)$$

where $g_{33}$ is a piezoelectric voltage constant for the case where the force $F_{Hi}$ is directed the same way as the PZT polarisation; $C$ is the cross-sectional area of the PZT; and $t$ is its layer thickness. In view of the above, the energy $E$ of the water waves given in Eq. (3) can be transferred as work done by the force $F_{Vi}$ in Eq. (6) and converted into a useful electrical form at a voltage $V_{Si}$ as shown in Eq. (7). This conversion takes place with efficiency $\eta_i$. The electrical form of energy obtained in this way can be used to power IoT devices.

## OSCILLATING BODY SYSTEM WAVE ENERGY CONVERTER

A wave energy converter was designed and constructed in the form of an oscillating body system, following the WECs classification [2]. It consisted of three-body heaving cylindrical buoys trapped in a fixed frame with an openwork structure. Each cylindrical buoy was 240 mm high and 65 mm in diameter, and had a mass of 80 g. The openwork frame was 160 mm wide, 130 mm deep, and 450 mm high. The openings of the openwork structure were 50 mm in diameter. All of the elements were made of polypropylene, and are illustrated in Fig. 3.

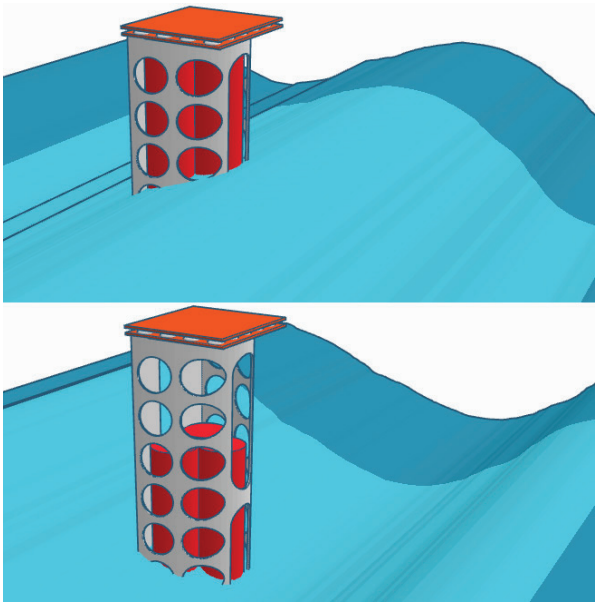

*Fig. 3. Wave energy absorber consisting of three body heaving cylindrical buoys (red) trapped in a fixed frame with an openwork structure (white) working in waves (top dead centre position on the top and bottom dead centre position on the bottom).*

The heaving buoys were intended to move with the motion of the water surface, and to act as a force on the PZT transducers fixed to the frame. The piezoelectric module was constructed in the form of 20 PZT/brass disk transducers, fixed to a common surface. The disk transducers consisted of PZT and brass plates, with diameters 19 mm (PZT) and 27 mm (brass) and an overall thickness of 0.24 mm. Each transducer had a capacitance of 45 nF, an impedance of 250 Ω and a resonant frequency of 2500 Hz. The PZT electrodes were led out with LgY0.5 wires with a stranded core structure and a core section of 0.5 mm$^2$. The brass plates were soldered to the common copper surface. The piezoelectric module is shown in Fig. 4.

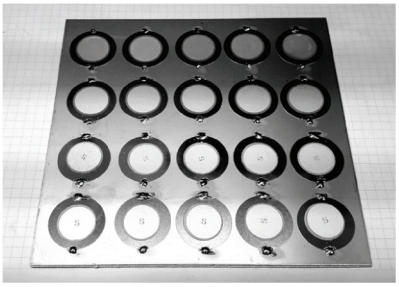

*Fig. 4. PZT converter, consisting of 20 PZT/brass disk transducers fixed to a common copper surface.*

The energy converted by the PZT into electrical form was further processed via a prototype power electronic circuit (PEC), as illustrated in the schematic diagram in Fig. 5.

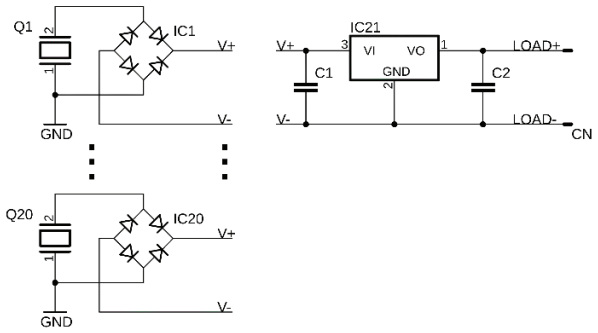


*Fig. 5. Schematic diagram of a prototype power electronic circuit consisting of PZT/brass disk transducers (Q1–Q20), full-wave single-phase bridge rectifiers (IC1–IC20), input capacitor C1, very low-dropout voltage regulator IC21, output capacitor C2, and male connector CN for the load.*

The implementation of the PEC is shown in Fig. 6. The system was constructed on a prototype PU26 universal board with a width of 60 mm, a height of 90 mm and a thickness of 1.6 mm.

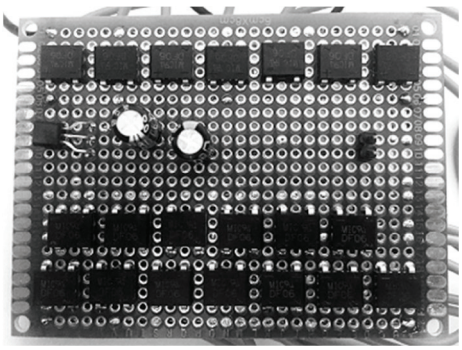

*Fig. 6. Implementation of the prototype power electronic circuit.*

The prototype board consisted of the components listed in Table 1.

*Table 1. Components of the prototype power electronic circuit.*

| Item | Reference | Description | Value | MPN [1] | Quantity |
|---|---|---|---|---|---|
| 1 | IC1–IC20 | Bridge recti-fiers | N/A | DF06 | 20 |
| 2 | IC21 | Voltage regula-tor | N/A | LE33 | 1 |
| 3 | C1 | Input capaci-tor | 10 µF | KE10/ 100 | 1 |
| 4 | C2 | Output capaci-tor | 47 uF | KE47/ 50 | 1 |
| 5 | CN | Male conne-ctor | N/A | 87220 -2 | 1 |

1 Manufacturer part number

In the operation of the PEC, the piezoelectric voltage of the PZT electrodes is full-wave rectified by single-phase bridges (IC1–IC20). The input capacitor (C1) of the very low-dropout voltage regulator (IC21) is then charged at the rectified voltage. Next, the output current of the IC21 charges the output capacitor (C2) at the voltage that is applied to the load. In this way, the load is powered with the harvested energy.

## INTERNET OF THINGS END NODE DEVICE

The IoT END considered under the present investigation consisted of a 2.71" e-paper display [21] and an STM32WL55JC ultra-low-power microcontroller with an embedded radio module enabling the LoRa modulation [22].

An electronic paper display (EPD), commonly referred to as an e-paper, is an electronic display that looks and feels similar to regular paper. EPDs contain microcapsules that are filled with electrically charged ink particles: black ink particles are negatively charged, while white ones are positively charged. Although colour EPDs are available, monochrome EPDs have lower power needs and are therefore considered in the current study. When an appropriate charge is applied to the display surface, it is possible to create very detailed images with similar contrast and legibility to those of traditional printing. The e-paper screen consumes electricity only when the displayed content changes, and once the ink particles are in place, they remain there for years. The details of e-paper technology have been thoroughly described by its manufacturer [21]. The 2.71" e-paper display used in the present study is shown in Fig. 7.

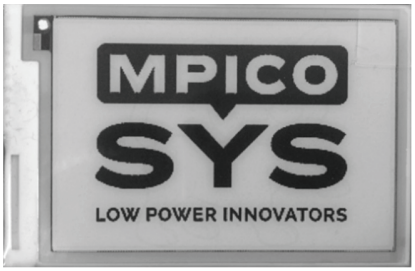


*Fig. 7. The 2.71" black and white e-paper display used in the present study, with an example of graphical content.*

The 2.71" display had an active area size of 57.3 × 38.2 mm, a resolution of 264 × 176 px, a density of 117 DPI, and a 2-bit colour depth, which corresponds to four shades of gray. Its visual similarity to regular paper can be seen in Fig. 8.

*LoRa* is a long-range, low-power wireless modulation technique. It is derived from chirp spread spectrum (CSS) technology and encodes information about radio waves using pulses (known as chirp pulses) in a manner similar to that used by dolphins and bats [24]. A modulated *LoRa* transmission is resistant to interference, and can be received over long distances of many kilometres. These distances can reach more than 22 km for transmission over seawater [25] or even more than 830 km for stratospheric balloons [26]. *LoRa*

is a solution used in applications that send small amounts of data, and these data can be transmitted over long distances compared to technologies such as Wi-Fi, Bluetooth or BLE, at relatively low digital transmission speeds. These features make *LoRa* well-suited to sensors and actuators that operate in a very low-power mode [24]. A comparison of *LoRa* with other selected wireless communication technologies in terms of bandwidth and range is presented in Fig. 9. The *LoRa* radio modules available on the market are characterised by very low power consumption, and are referred to by manufacturers as ultra-low-power solutions [22]. *LoRa* can operate in licence-free sub-gigahertz bands, such as at 915, 868, and 433 MHz. It can also operate in the 2.4 GHz band to achieve higher data rates compared to sub-gigahertz bands, at the cost of a lower range. These frequencies belong to the ISM bands, which are reserved worldwide for industrial, scientific, and medical purposes [24].

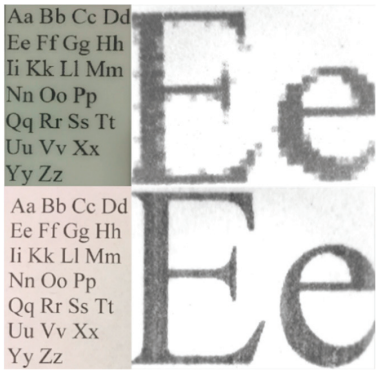


*Fig. 8. Top image: 2.71" vertically oriented display; bottom image: regular paper. A normal view is shown on the left and a 50× magnification using a USB Delta Optical DO Smart microscope on the right.*

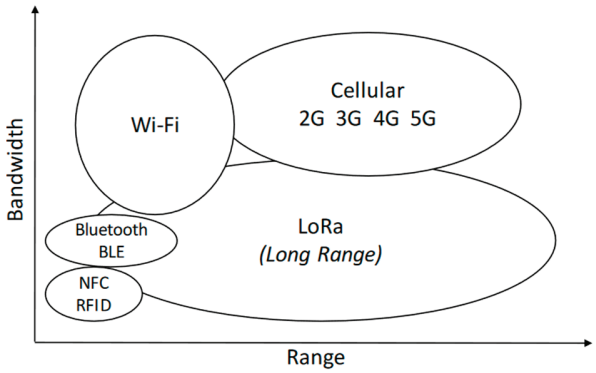


*Fig. 9. Comparion of LoRa with other selected wireless communication technologies in terms of bandwidth and range.*

Our experimental *LoRa* setup consisted of a *The Things Indoor Gateway* based on a Semtech SX1308 chipset and an end node based on the STM32WL55JC microcontroller. The transmission power of the gateway was 27 dBm, corresponding to 500 mW, and its receiving sensitivity was –140 dBm. The transmission power of the end node radio module was 15 dBm, corresponding to 32 mW, and its receiving sensitivity was –148 dBm. The time on air was 0.4 s, meaning that a duty cycle of longer than 40 s was required to maintain 1% time on air. A frequency of 868 MHz was used.

An IoT END prototype was developed, re-constructed to operate with the STM32WL55JC microcontroller, and researched by the author in cooperation with the MpicoSys Embedded Pico Systems (MpicoSys) company. This IoT END module is commercially offered and produced by MpicoSys, a company that provides complete solutions in the field of design, engineering, production, and rapid prototyping of e-paper for ultra-low-power and no-power technologies [27]. The IoT END device used in this study, in the form of an air quality indicator made of e-paper, is shown in Fig. 10. The device displays the results of air quality measurements at a station in Gdynia, Poland. These measurements are shared online by the Chief Inspectorate of Environmental Protection and acquired by the IoT END via *LoRa* communication.

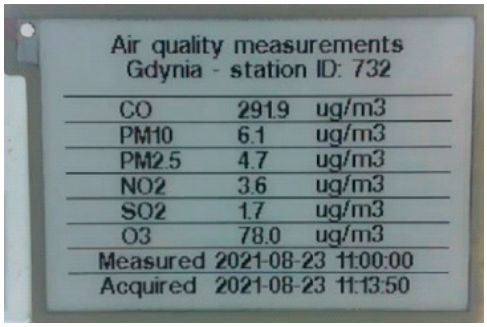


*Fig. 10. IoT END device in the form of an air quality indicator made of e-paper.*

## EXPERIMENTAL RESEARCH

Our research consisted of a set of physical experiments. Two series of measurements were carried out to enable us to compare the results for the energy consumed by the IoT END with the energy supplied by the WEC. These measurements were carried out separately, and the results were compared.

The energy consumption of the IoT END was investigated in one of the possible use cases. The use case was considered in accordance with one of the solutions developed by the author and offered on the market by MpicoSys. The scenario included periodic data acquisition and refreshing of the display with user-directed information on air quality. The data were acquired and refreshed every 10 minutes, and the information displayed on the IoT END was acquired over *LoRa*. The IoT END consisted of two elements that consumed energy: a 2.71" EPD, and a STM32WL55JC microcontroller enabling the *LoRa* modulation. The STM32WL55JC microcontroller was equipped with firmware that performed low-power functions, and which received the data via the *LoRa* communication. Both of these elements were powered by DC voltage and consumed varying current depending on their needs, which was measured using an Otii Arc energy consumption analysis tool. Measurements were made over the *LoRa* communication cycle including the reception of 215 bytes of data and the

idle state and full refresh of the 2.71-inch EPD. A sampling frequency of 1 kHz and a resolution of 2.5 μA were used. Measurements of the current were performed at a DC supply voltage of 3.3 V set in the Otii Arc.

The energy supplied by the WEC was investigated in one possible application case. It can be mounted on breakwaters, piers, piles or other coastal structures. In the use case, it was assumed that the WEC would be positioned in a coastal zone where waves break and turbulise, meaning that the mechanical impacts have a higher frequency that is particularly suitable for piezoelectric materials such as PZT, due to their relatively high resonant frequency. The wave energy absorber of the WEC was submerged in a test tank at a depth of 30 cm, as shown in Fig. 11.

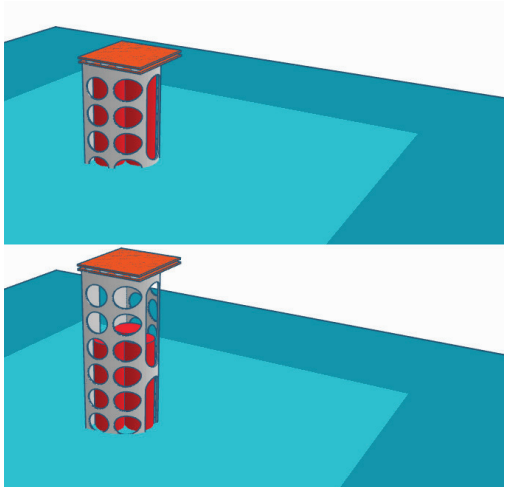

*Fig. 11. The wave energy absorber submerged in water in a test tank – top dead centre position on the top and bottom dead centre position on the bottom.*

The construction of the PZT converter and the mechanical bumpers before assembly is shown in Fig. 12. Mechanical bumpers were needed as interlayers between the impact surface of the buoy and the PZT. Each bumper was 13 mm in diameter, 5 mm thick and made of polyvinyl chloride.

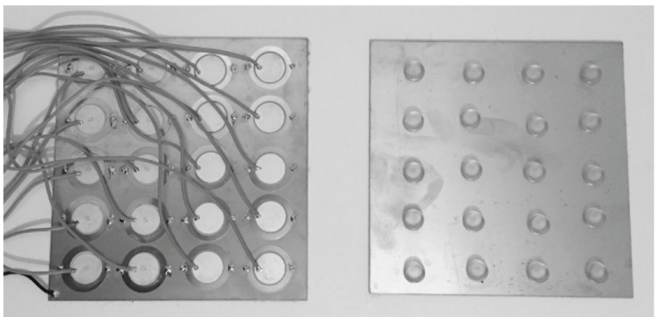

*Fig. 12. View before assembly: PZT converter (left); mechanical bumpers (right)*

The components shown in Fig. 12 were assembled as shown in Fig. 13.

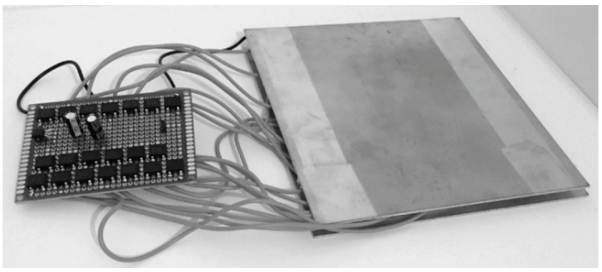

*Fig. 13. After assembly: PZT converter and mechanical bumpers, connected to the power electronic circuit.*

After assembly with the mechanical bumpers, the PZT converter was attached to the top of the wave energy absorber for the duration of the measurements, meaning that the vertical force from the moving buoys acted on the PZT. From Eq. (7) and considering that the vertical force is involved in energy conversion, the equivalent of the formation of waves on the water surface was the heaving of the WEC absorber relative to the water surface. Consequently, the WEC was heaved up and down into the water to model the action of the force. The vertical movements were performed at a frequency corresponding to the wave whose vertical action was modelled. The energy supplied by the WEC was measured using an STM32F429ZIT6U microcontroller equipped with firmware to perform the analogue-to-digital (ADC) conversion of the voltage acquired from the LOAD+ and LOAD- output terminals (Fig. 5). The measured voltage acquired and processed using a 12-bit ADC converter was subsequently sent to the RS232 terminal of the personal computer via the UART interface and recorded. A sampling frequency of 25 Hz was used, with a resolution of 0.732 mV. Measurements of the generated voltage were made with a 2.94 kΩ load resistor connected to the LOAD+ and LOAD- WEC output terminals, and the results from the generated voltage with a fixed load resistance allowed us to calculate the current flowing in the circuit and hence the energy generated by the WEC.

In the case study considered here, important messages (such as air or water quality, alerts or weather forecasts) could be transmitted in coastal areas via long-range wireless communication using wave energy. It was essential to ensure that the energy produced by WEC exceeded the energy consumed by the IoT END for this application. The results are presented and discussed in the following section.

## RESULTS

According to research performed on the IoT END and described in this paper, the STM32WL55JC microcontroller handling the *LoRa* modulation consumed an average current of 684 μA. This current consumption occurred at a supply voltage of 3.3 V DC during one *LoRa* communication cycle in which 215 B of data were received. This is shown in Fig. 14 over the time period 0.2–5.7 s.

The STM32WL55JC microcontroller consumed an average current of 2.42 μA in the idle state at a supply voltage of

3.3 V DC. This is shown in Fig. 14 over the time period 5.7–10 s.

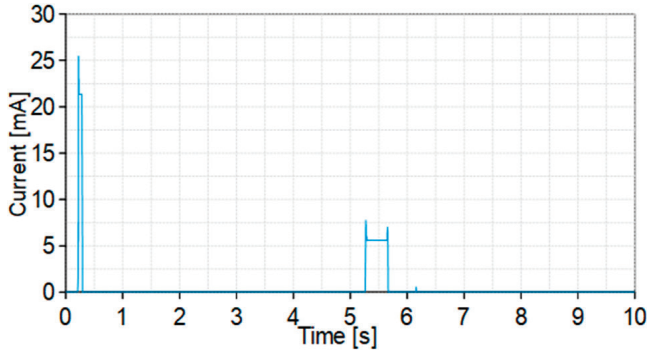


*Fig. 14. Current consumed by the STM32WL55JC at a supply voltage of 3.3 V DC, showing the LoRa communication cycle receiving 215 B of data from 0.2 to 5.7 s, and the idle state from 5.7 to 10 s, measured using Otii Arc.*

The 2.71" EPD consumes an average current of 1.72 mA at a supply voltage of 3.3 V DC during the update cycle when the display is refreshed. It is shown in Fig. 15 over the time period 0.1–1.7 s.

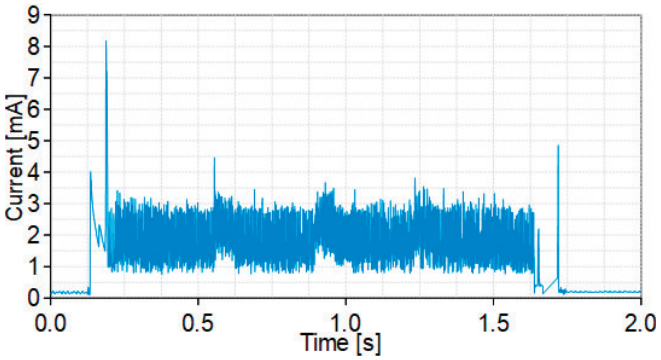


*Fig. 15. Current consumed by the 2.71" EPD at a supply voltage of 3.3 V DC, showing the display update cycle (when the display area of 264 ×176 px is refreshed) between 0.1 and 1.7 s.*

A summary of the energy consumed by the IoT EPD for the use case considered here, for a data acquisition and display refresh cycle of 10 min, is presented in Table 2.

*Table 2. Summary of IoT EPD energy consumption for one data acquisition/ display update cycle*

| State | Average current[1] [μA] | Period[2] [s] | Energy consumption [mJ] |
|---|---|---|---|
| Idle | 2.42 | 592.9 | 4.74 |
| Communication | 684 | 5.5 | 12.42 |
| Display update | 1720 | 1.6 | 9.08 |
| Total | N/A | 600 | 26.23 |

[1] For a supply voltage of 3.3 V DC

[2] For a data acquisition and display update period of 10 min

From these results, it can be seen that the energy consumption of the IoT END over one 10 min period of data acquisition via *LoRa* and display update was equal to 26.23 mJ.

The experiments performed on the WEC showed that the converter supplied an average current of 90 μA at an average voltage of 263 mV, generated under the impact of a vertical force resulting from a modelled wave with a height of 30 cm and a frequency of 1.3 Hz. These conversion parameters were found for a load with a 2.94 kΩ resistor. The mean values reported here were calculated from the pulsating value of the generated voltage measured at the WEC output terminals (Fig. 5). The results of the generated voltage measurements are shown in Fig. 16.

An amplitude of 30 cm for the vertical movement was measured on a centimetre measuring scale. The frequency of 1.3 Hz for the vertical movement was measured and registered (it corresponded to the frequency of the WEC's voltage generated).

The wave frequency of 1.3 Hz was chosen as an optimum trade off between the harmonic energy density of natural water waves and their high dynamics, desirable for the PZT element. Based on the classification of ocean waves in terms of their frequencies [28], a harmonic value of 1.3 Hz corresponds to the region of wind sea waves, whereas higher frequencies correspond to the region of capillary waves. Since the energy density decreases from the wind wave region to the capillary wave region, a higher harmonic energy density would be too low for harvesting. The geometric dimensions of the WEC were selected to ensure that it was compact and easy to use for harvesting the energy of breaking waves and turbulised water near offshore, onshore and coastal structures.

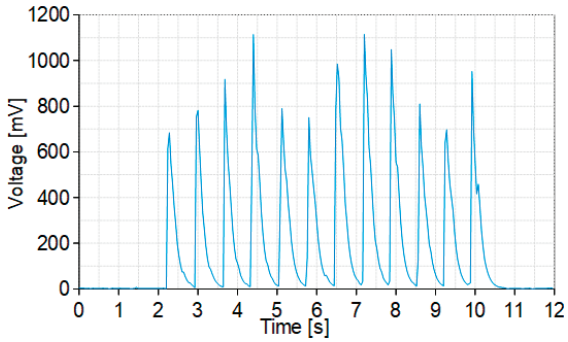


*Fig. 16. Measured voltage generated at the output terminals of the WEC under a load and force resulting from the modelled vertical impact of a water wave with a height of 30 cm at a frequency of 1.3 Hz.*

The pulsating current was calculated for the known value of the load resistor, and the results are shown in Fig. 17.

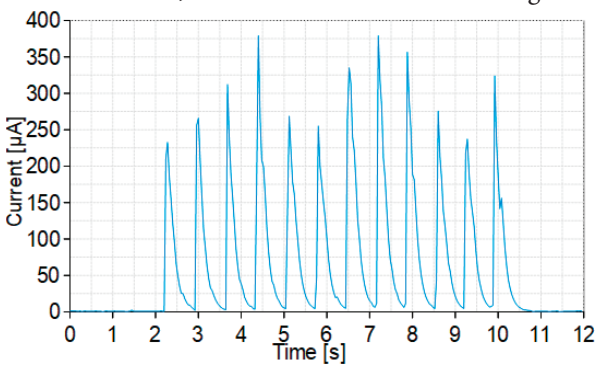


*Fig. 17. Current supplied to the output terminals of the WEC at a voltage generated under a load and force resulting from the modelled vertical impact of a water wave with a height of 30 cm at a frequency of 1.3 Hz.*

The variation in the power was then calculated for the known values of the voltage and current, and the results are shown in Fig. 18.

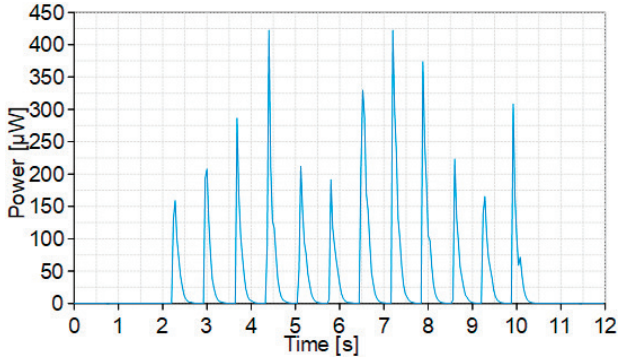


*Fig. 18. Power supplied from the WEC to the load under the force resulting from the modelled vertical impact of a water wave with a height of 30 cm at a frequency of 1.3 Hz.*

From the 12-s measurement gates presented in Figs. 16, 17, and 18, a time range from 2.2 to 10 s was considered for further analysis, which corresponded to the active impact of the modelled wave.

A summary of the energy conversion performance of the WEC under the applied load and the modelled impact of the wave is presented in Table 3.

*Table 3. Summary of WEC energy conversion performance under the load and the modelled impact of the wave*

| Parameter | Average value[1] | Units |
|---|---|---|
| Voltage | 263 | mV |
| Current | 90 | μA |
| Power | 51 | μW |
| Energy[2] | 30.3 | mJ |
| Load | 2.94 | kΩ |
| Wave height | 30 | cm |
| Wave frequency | 1.3 | Hz |

1 Average value from 2.2 s to 10 s

2 For the 10-min IoT END period

The results show that the amount of the energy converted into electrical form was 30.3 mJ, whereas the amount of energy consumed by the IoT END was 26.23 mJ. Both of these values correspond to one cycle of data acquisition and display updating for the IoT END over a 10 min period.

The output power of the IoT END transmitter reached up to 32 mW. The power generated by the WEC was of 51 μW. However, the transmission time was short enough to balance the energy consumption and generation. Our experimental results confirmed that an energy surplus was supplied by the WEC compared to the energy consumption of the IoT END, indicating that wireless and mobile communication could be powered by freely available sea wave energy.

Balancing the energy generated and consumed requires the use of energy storage elements such as capacitors or micro-supercapacitors. The selection and validation of reliable energy storage elements will be performed in future work.

The piezoelectric voltage constant $g_{33}$ resulting from the material dimensions of the piezoelectric and the design of the wave energy absorber both have a significant impact on the parameters of energy conversion and WEC performance. Optimisation of the piezoelectric material and the wave energy absorber falls outside the scope of the present study, and will be considered in future work.

## DISCUSSION OF MARINE AREAS

The use case presented here for the proposed WEC was analysed for use in selected marine coastal areas. This study was conducted using information from the EU Copernicus Marine Service [29], and an analysis was performed using acquired values for the:

- Significant height of sea surface waves $H_{s,}$
- Period of sea surface waves at a variance spectral density maximum $T_p$.

The significant height $H_s$ is the average height of the highest one-third of the waves. The sea surface wave period at variance spectral density maximum $T_p$ is also known as the modal period or the peak period.

Data from 19th February 2023 were acquired for the following marine coastal areas, in alphabetical order:

1. Algeria, Bay of Algiers: 36.797N, 3.128E;
2. Estonia, Tallinn: 59.492N, 24.734E;
3. Finland, Oulu: 65.129N, 25.204E;
4. France, Dunkirk: 51.139N, 2.308E;
5. Israel, Haifa: 32.836N, 34.963E;
6. Japan, Hamamatsu: 34.636N, 137.748E;
7. Lithuania, Klaipeda: 55.652N, 21.076E;
8. Netherlands, Hague: 52.666N, 4.562E;
9. Norway, Trondheim: 64.294N, 10.373E;
10. Poland, Gdańsk Bay: 54.460N, 18.628E;
11. Poland, Jastrzębia Góra: 54.846N, 18.299E;
12. Poland, Międzyzdroje: 53.937N, 14.429E;
13. South Africa, Cape of Good Hope: 34.358S, 18.470E;
14. Sweden, Malmo: 55.629N, 12.979E;
15. United Arab Emirates, Dubai: 25.242N, 55.242E;
16. United Kingdom, Kingsbridge: 50.279N, 3.904W;
17. United States of America, California, San Francisco: 37.761N, 122.539W.

To carry out an energy analysis based on the values acquired from the global wave system, the relationship between the energy contained in the water waves and $H_s$ needed to be obtained as follows.

An expression for the amplitude spectrum harmonics $Z_{Ai}$ in terms of the power spectrum harmonics $S_i$ is given in Eq. (8):

$$S_i = \frac{1}{2} z_{Ai}{}^2 \tag{8}$$

Following [30], $H_s$ can be related to the power spectrum harmonics $S_i$ as shown in Eq. (9):

$$H_S = 4\sqrt{\sum_{i=1}^{\infty} S_i} \tag{9}$$

By substituting Eq. (8) into Eq. (9) and simplifying the equation, an expression for $Z_{Ai}$ can be formulated as shown in Eq. (10):

$$\sum_{i=1}^{\infty} z_{Ai} = \frac{1}{\sqrt{8}} H_S \tag{10}$$

We combine Eqs. (10) and (3) to find the energy $E$ expressed per unit of the water surface and contained in the water waves in terms of $H_s$, as shown in Eq. (11):

$$E = \frac{1}{16}\rho g {H_s}^2 \tag{11}$$

Using the equation given above, values for $E$ were calculated as listed in Table 4. The parameter $\rho$ was set to 998.7739 kg/m$^3$, and g was assumed to be equal to the standard value of 9.80665 m/s$^2$ in for the calculations. The value of $\rho$ corresponds to an average annual temperature of the surface waters of the oceans of 17°C.

*Table 4. Energy contained in water waves and expressed per unit of surface area of water for selected marine coastal areas*

| Coastal area[1] | $H_s$ [m] | $T_p$ [s] | $f_p$ [Hz] | $E$ [J/m$^2$] |
|---|---|---|---|---|
| 1 | 0.21 | 3.78 | 0.26 | 27 |
| 2 | 0.82 | 7.25 | 0.14 | 412 |
| 3 | 0.11 | 1.86 | 0.54 | 7 |
| 4 | 1 | 4.72 | 0.21 | 612 |
| 5 | 0.31 | 2.82 | 0.35 | 59 |
| 6 | 1.59 | 8.27 | 0.12 | 1548 |
| 7 | 1.5 | 6.39 | 0.16 | 1377 |
| 8 | 1.05 | 5.82 | 0.17 | 675 |
| 9 | 3.62 | 10.91 | 0.09 | 8022 |
| 10 | 0.78 | 6 | 0.17 | 372 |
| 11 | 0.98 | 5.58 | 0.18 | 588 |
| 12 | 0.67 | 3.91 | 0.26 | 275 |
| 13 | 1.62 | 12.06 | 0.08 | 1607 |
| 14 | 0.56 | 3.39 | 0.29 | 192 |
| 15 | 1.49 | 7.11 | 0.14 | 1359 |
| 16 | 0.8 | 12.4 | 0.08 | 392 |
| 17 | 1.06 | 12.12 | 0.08 | 688 |

[1] Numbering follows the list of marine coastal areas in alphabetical order given above

The solution presented in the previous sections ensured that the energy supplied by the WEC exceeded the energy consumed by the IoT END. This amount of energy was generated under the vertical impact of a modelled water wave with height 30 cm and frequency 1.3 Hz. The energy contained in this water wave was 441 J/m$^2$, a value calculated using Eq. (1). The parameter ρ was set to 999.6991 kg/m$^3$ and g was taken as the standard value of 9.80665 m/s$^2$ for the calculations. This value of ρ corresponds to a water temperature of 10°C in the test tank.

The WEC converted the energy of the wave at a frequency of 1.3 Hz, corresponding to a period of 0.77 s. The value of Tp found for the data acquired from the global wave system ranged from 1.86 s to 12.4 s. However, the proposed WEC is intended to be mounted on nearshore coastal structures, where the waves break and turbulise, and the local wave period is therefore expected to increase significantly, meaning that the mechanical impact is expected to have a higher frequency, closer to the tested value of 1.3 Hz.

The topology of the coastal structures and the presence of wave breakers or turbulisers have a significant impact on the parameters of a broken wave; however, this type of breaking falls outside the scope of the present study, and will be considered in future work.

Our energy analysis based on data acquired for 19th February 2023 show that the use of the IoT END with the proposed WEC is suitable for coastal areas 4, 6, 7, 8, 9, 11, 13, 15, 17. For coastal areas 1, 2, 3, 5, 10, 12, 14, 16, the update period of the IoT END needs to be extended to allow the generated energy to exceed that consumed by the IoT END.

## CONCLUSIONS

The use of the proposed WEC to power an IoT device was successfully verified for the case study considered here. The perovskite-based WEC designed and constructed as part of this study was experimentally proven to be capable of generating the energy required by distributed and autonomous IoT ENDs. In the event of insufficient wave energy, the update period for the IoT END can be extended to allow the generated energy to exceed the IoT END energy consumption. The solution presented here can make significant contributions to the sustainable development of wireless and mobile communication powered by freely available sea wave energy.

The main advantage of our technical solution compared to existing alternatives is that it is very compact and can harvest energy directly at the point where it is consumed by the distributed, autonomous elements of an IoT network located onshore, nearshore, or offshore. A further advantage over related schemes introduced in recent years [4] is that the proposed solution uses an innovative method of energy conversion based on PZT ceramic perovskite material. In addition, other related systems are based on electrical machines that require maintenance, whereas the solution proposed in this paper uses maintenance-free piezoelectric materials. This feature is a particular advantage for a distributed, energy-autonomous IoT network operating in marine conditions.

In future research, we intend to consider and implement optimised piezoelectric materials and a wave energy absorber to improve the performance of the WEC. Further research will also be carried out to match the piezoelectric materials

to the frequency of water waves, and to apply a matching inductance to the piezoelectric circuit, which will increase the efficiency of the water wave energy conversion. In future, it will also be useful to analyse the topology of coastal structures, wave breakers or turbulisers and their impacts on the wave energy conversion parameters. In further work to extend the current scheme, the experimental system will be tested and demonstrated in real environments.

## REFERENCES


1. P. Girard and S. Girard, Brevet D'invention De Quinze Ans, "Pour divers moyens d'employer les vagues de la mer, comme moteurs," a patent for invention, Paris 1799, 349.

2. T. Aderinto and H. Li, "Ocean wave energy converters: Status and challenges," Energies, vol. 11, p. 1250, 2018. doi:/10.3390/en11051250.

3. A. Clément et al., "Wave energy in Europe: Current status and perspectives," Renewable and Sustainable Energy Reviews, vol. 6, p. 5, 2002. doi:10.1016/S1364-0321(02)00009-6.

4. M. S. Lagoun, A. Benalia, and M. E. H. Benbouzid, "Ocean wave converters: State of the art and current status," Proceedings of the 2010 IEEE ENERGYCON, Manama (Bahraïn), December 2010, pp. 636–642.

5. A. Maria-Arenas et al., "Control strategies applied to wave energy converters: State of the art," Energies, vol. 12, p. 3115, 2019. doi:10.3390/en12163115.

6. M. A. Jusoh et al., "Hydraulic power take-off concepts for wave energy conversion system: A review," Energies, vol. 12, p. 4510, 2019. doi:10.3390/en12234510.

7. S. Chiba et al., "Consistent ocean wave energy harvesting using electroactive polymer (dielectric elastomer) artificial muscle generators," Applied Energy, vol. 104, pp. 497–502, 2013. doi:10.1016/j.apenergy.2012.10.052.

8. X. Chou et al., "All-in-one filler-elastomer-based high-performance stretchable piezoelectric nanogenerator for kinetic energy harvesting and self-powered motion monitoring," Nano Energy, vol. 53, pp. 550–558, 2018. doi:10.1016/j.nanoen.2018.09.006.

9. M. Weiser, "The computer for the 21st century," Scientific American, vol. 265, pp. 94–104, 1991.

10. R. Qiu and Z. Zhang, "Design of enterprise Web servers in support of instant information retrievals," IEEE RFID Virtual Journal, pp. 2661-2666, vol. 3, 2003. doi:10.1109/ICSMC.2003.1244286.

11. M. H. Miraz et al., "A review on Internet of Things (IoT), Internet of Everything (IoE) and Internet of Nano Things (IoNT)," IEEE Spectrum, pp. 219–224, 2015. doi:10.1109/ITechA.2015.7317398.

12. T. Hiramoto et al., "Ultra-low power and ultra-low voltage devices and circuits for IoT applications," IEEE Silicon Nanoelectronics Workshop (SNW), pp. 146–147, 2016. doi:10.1109/SNW.2016.7578025.

13. S. K. Vishwakarma et al., "Smart energy efficient home automation system using IoT," IEEE 4th International Conference on Internet of Things: Smart Innovation and Usages (IoT-SIU), pp. 1–4, 2019. doi:10.1109/IoT-SIU.2019.8777607.

14. K. Wasa, et al., "Thin films of PZT-based ternary perovskite compounds for MEMS," IEEE Ultrasonics Symposium, pp. 213–216, 2008. doi:10.1109/ULTSYM.2008.0052.

15. J. Dudziak, "Dynamika środowiska," in Teoria okrętu, Wydawnictwo Morskie, Gdańsk, Poland, 1988, p. 338 (in Polish).

16. A. Iafrati et al., "Laboratory modelling of waves: Regular, irregular and extreme events," in Proceedings of the Specialist Committee on Modeling of Environmental Conditions, 28th ITTC, Wuxi, China, 17–22 September 2017, p. 8.

17. C. T. Stansberg et al., "Final report and recommendations to the 23rd ITTC," in Proceedings of the 23rd ITTC, Volume II, Specialist Committee on Waves, Venice, Italy, 8–14 September 2002, p. 517, pp. 544–551.

18. G. G. Cox et al., "Report of the Seakeeping Committee," in Proceedings of the 17th ITTC, Volume I, Seakeeping Committee, 17th ITTC, Goteborg, Sweden, 8–15 September 1984, p. 482.

19. M. Drzewiecki and J. Guziński, "Fuzzy control of waves generation in a towing tank," Energies, vol. 13, p. 2049, 2020. doi:10.3390/en13082049.

20. APC International, Ltd., "Modes of vibration for common piezoelectric ceramic shapes," in Piezoelectric Ceramics: Principles and Applications, APC International, Ltd.: Mackeyville, PA, USA, 2011, Table 1.8.

21. Pervasive Displays 2.71" E-ink display. Accessed: Feb. 11, 2023 [Online]. Available: https://www.pervasivedisplays.com/product/2-71-e-ink-display/

22. STM32WL55JC Sub-GHz Wireless Microcontrollers. Dual-core Arm Cortex-M4/M0+ @48 MHz with 256 Kbytes of Flash memory, 64 Kbytes of SRAM. LoRa, (G)FSK, (G)MSK, BPSK modulations. AES 256-bit. Multiprotocol System-on-Chip. Accessed: Feb. 11, 2023). [Online] Available:

https://www.st.com/en/microcontrollers-microprocessors/stm32wl55jc.html

23. Pervasive Displays, "How low-power e-paper displays enhance IoT applications." Accessed Feb. 11, 2023. [Online]. Available: https://www.pervasivedisplays.com/how-e-paper-works/

24. The Things Network, "What are LoRa and LoRaWAN?" Accessed Feb. 11, 2023. [Online]. Available: https://www.thethingsnetwork.org/docs/lorawan/what-is-lorawan/

25. N. Jovalekic et al., "Experimental study of LoRa transmission over seawater," Sensors, vol. 18, p. 2853, 2018. doi: 10.3390/s18092853.

26. The Things Network Global Team, "LoRaWAN® distance world record broken, twice." Accessed Feb. 11, 2023. [Online]. Available: https://www.thethingsnetwork.org/article/lorawan-world-record-broken-twice-in-single-experiment-1

27. "MPICOSYS Low Power Innovators Invent, Design & Produce For You." Accessed Feb. 11, 2023. [Online]. Available: https://www.mpicosys.com/

28. L. H. Holthuijsen, Waves in Oceanic and Coastal Waters. Cambridge: Cambridge University Press, 2007, p. 4.

29. Copernicus Marine Service Information, "Global Ocean Waves Analysis and Forecast," doi:10.48670/moi-00017. Accessed Feb. 19, 2023. [Online]. Available: https://data.marine.copernicus.eu/product/GLOBAL_ANALYSISFORECAST_WAV_001_027/description

30. P. Gualeni et al., "Confidence intervals for significant wave height and modal period," In Recommended Procedures and Guidelines, Specialist Committee on Stability in Waves of the 28th ITTC, Wuxi, China, 17–22 September 2017, p. 4.